J. Fluid Mech. (2020), *vol.* 896, R2, doi:10.1017/jfm.2020.394

JFM RAPIDS
journals.cambridge.org/rapids

Deformation upon impact of a concentrated suspension drop

Loren Jørgensen[1], **Yoël Forterre**[1] **and Henri Lhuissier**[1,†]

[1]Aix Marseille Université, CNRS, IUSTI, Marseille, France

(Received 24 March 2020; revised 7 May 2020; accepted 12 May 2020)

We study the impact between a plate and a drop of non-colloidal solid particles suspended in a Newtonian liquid, paying specific attention to the case when the particle volume fraction, ϕ, is close to – or even exceeds – the critical volume fraction, ϕ_c, at which the steady effective viscosity of the suspension diverges. We use a specific concentration protocol together with an accurate determination of ϕ for each drop, and we measure the deformation β for different liquid viscosities, impact velocities and particle sizes. At low volume fractions, β is found to follow closely an effective Newtonian behaviour, which we determine by documenting the low-deformation limit for a highly viscous Newtonian drop and characterizing the effective shear viscosity of our suspensions. By contrast, whereas the effective Newtonian approach predicts that β vanishes at ϕ_c, a finite deformation is observed for $\phi > \phi_c$. This finite deformation remains controlled by the suspending liquid viscosity and increases with increasing particle size, which suggests that the dilatancy of the particle phase is a key factor in the dissipation process close to and above ϕ_c.

Key words: suspensions, drops, particle/fluid flow

1. Introduction

The collision between a particle-laden drop and a solid is encountered in many natural situations or industrial applications, such as spore dispersal (Ingold 1971) or inkjet printing of colloidal particle drops for microelectronics (Korkut, Saville & Aksay 2008; Qi *et al.* 2011) and microfabrication (Derby 2011). It is, however, a challenging problem, which couples the dynamics of a highly unsteady free surface flow with the complex rheology of particulate suspensions. For a Newtonian liquid, the impact dynamics may involve capillarity or the influence of ambient air, but for a sufficiently viscous medium, the deformation of the drop is controlled only by a balance between the drop initial kinetic energy and bulk dissipation (Madejski 1976; Chandra & Avedisian 1991; Laan *et al.* 2014; Josserand & Thoroddsen 2016;

† Email address for correspondence: henri.lhuissier@univ-amu.fr

Wildeman *et al.* 2016; Gordillo, Sun & Cheng 2018). This overdamped limit may seem relevant for the impact of a drop containing a large quantity of solid particles, since the bulk effective viscosity of a particulate suspension increases strongly with increasing volume fraction and eventually diverges at the critical volume fraction $\phi_c \approx 0.60$ (Zarraga, Hill & Leighton 2000; Stickel & Powell 2005; Guazzelli & Pouliquen 2018). However, depending on the preparation protocol, the particle volume fraction of a suspension can actually exceed ϕ_c. In such a case, the effective viscosity is undefined and it remains unclear how much an impacting drop spreads for $\phi > \phi_c$, as well as whether an effective Newtonian approach is relevant when ϕ becomes close to ϕ_c or what is the influence of the particle size.

So far, the limit of high volume fractions have been studied mostly for suspensions of small particles subjected to colloidal forces, which eventually shear-thicken (Bertola & Haw 2015; Boyer *et al.* 2016), or to document the capillary limited spreading and splashing for non-neutrally buoyant particles (Peters, Xu & Jaeger 2013; Lubbers *et al.* 2014; Grishaev *et al.* 2015; Schaarsberg *et al.* 2016; Raux *et al.* 2020). To our knowledge, the viscous spreading of drops of non-colloidal particles has only been studied up to intermediate volume fractions ($\phi < 0.45$) with an effective Newtonian approach assuming a large deformation of the drop (Nicolas 2005). The viscous spreading of a highly concentrated suspension drop has thus remained an open question, which is precisely the concern of this paper. We tackle the question by focusing on high-velocity impacts (large Froude and Weber numbers, i.e. large inertial stresses relative to gravitational and capillary stresses) and overdamped spreadings and studying the early dynamics during which the initial kinetic energy of the drop is dissipated (i.e. before any slower gravitational/capillary relaxation occurs).

In § 2, we present the experimental protocol used to prepare and impact highly concentrated drops, as well as first observations for various volume fractions, impact velocities and viscosities. In § 3, we analyse these results in the framework of a viscous effective modelling of the suspension, which is calibrated with experiments on Newtonian drops. Some crucial limitations of the effective viscosity approach are evidenced for particle volume fractions close to or above ϕ_c, which are discussed in terms of granular dilatancy effects and their coupling with the liquid pore pressure (§ 4). Finally, our conclusions are summarized in § 5.

2. Experimental set-up and general observations

2.1. *Set-up*

The drop impact protocol is sketched in figure 1. It consists in letting a suspension drop fall and impact perpendicularly onto a plate and observing the first milliseconds following the impact, during which the kinetic energy is dissipated.

The suspensions are prepared by immersing spherical polystyrene particles (Dynoseed TS, Microbeads, with a density of 1049 kg m^{-3}) in a Newtonian liquid with a close density. Most of the experiments are performed with a mean particle diameter $d = 145$ µm and a relative standard deviation in size below 4 %. A larger diameter ($d = 585$ µm $\pm$ 1 %) is also used (see § 4). These 'large' particle sizes ensure that interparticle forces are negligible (Morris 2020) and that the suspensions do not shear-thicken (which we have also verified, for $d = 145$ µm and up to $\phi = 0.50$, during the rheological characterization of the suspensions presented in § 3.2). The liquid is a water solution of PEGPG (3.9 kg mol^{-1} poly(ethylene glycol-*ran*-propylene glycol)-monobutylether by Sigma-Aldrich), which wets the particles well (the contact angle is typically smaller than 45°) and is sufficiently viscous to avoid particles being

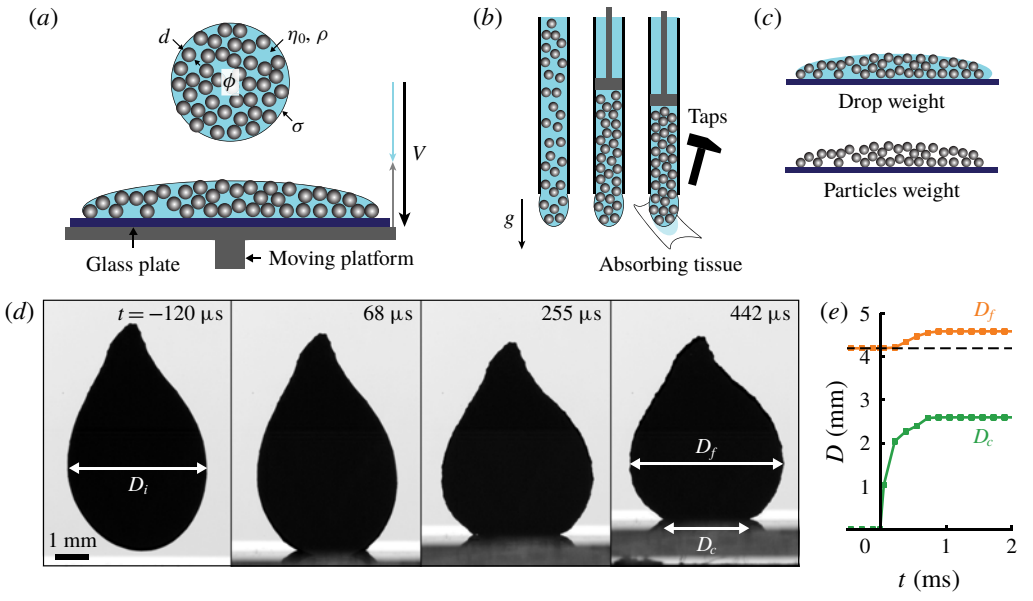

FIGURE 1. (*a–c*) Schematics of (*a*) the impact set-up, (*b*) the concentrated drop production method and (*c*) the post-impact measurement of the particle volume fraction. (*d*,*e*) Spreading dynamics and temporal evolution of the drop diameter for a drop with a particle volume fraction $\phi = 0.556$ and an impact velocity $V = 4$ m s^{-1} ($d = 145$ µm, $\eta_0 = 50.5$ mPa s, $\rho V D_i/\eta_0 = 350$, $t = 0$ indicates the instant of contact).

ejected from the drop during impact. Its viscosity, η_0, is varied between 0.93 and 192 mPa s by adjusting the PEGPG concentration (from 0 to 50 wt %), whereas its density and surface tension vary from 998 to 1056 kg m^{-3} and from 70 to 40 mN m^{-1}, respectively.

The particle volume fraction of the drop, ϕ, is varied from 0 to above the critical volume fraction. For moderate concentrations ($\phi \leqslant 0.54$), the formation of the drop is straightforward. The suspension is prepared at the desired ϕ, infused in a truncated (nozzle-free) plastic syringe with an inner diameter of 4.6 mm and the suspension is slowly extruded until the drop detaches. For $\phi < 0.54$, this simple protocol ensures that the volume fraction in the drop is identical (within less than 0.01, as verified *a posteriori*) to the nominal volume fraction of the preparation. However, it does not allow one to control and reproduce the solid content for more concentrated drops. Those drops, with $\phi > 0.54$, are thus obtained by infusing a suspension with a volume fraction of $\approx$0.55 in the syringe and concentrating each drop inside the syringe, by letting the particles sediment under gentle tapping or soaking part of the liquid with an absorbing tissue (see figure 1*b*). In this case the value of ϕ is determined post-impact by weighing, for each single drop, both the whole drop and its dry content obtained after washing and drying the particles. This protocol permits volume fractions as high as 0.62 to be reached, with an uncertainty of less than 0.005. The most concentrated drops (above $\phi_c \simeq 0.605$) behave like a paste. To avoid them extruding as a long cylinder, their shape is progressively relaxed by gently tapping the syringe. The detached drops remain oblong (see figure 1*d*) and care is taken to discard the impacts for which the drop has rotated.

The drop impacts a smooth glass plate (washed and rinsed with micro-filtered water before each impact). However, a series of impacts has also been performed on a rough surface (flat sand paper with a grain size $\approx 160\ \mu\text{m} \approx d$) to verify the influence of potential sliding of the particles on the surface (see § 2.2). The impact velocity V is varied from 1.6 to 10 m s^{-1}. In order to achieve the largest velocities while keeping aerodynamic effects on the drop negligible, the drop is released from a small height ($\approx$20 cm) and the plate is moved vertically towards the drop. To this end, the plate is stuck on a fast translating stage (electromagnetic actuator, Copley STA2506S). The stage motion is triggered by the occulting of a laser beam by the falling drop and the displacement versus time law is tuned so as to ensure that the impact occurs at the fixed observation spot with the desired impact velocity V ($= |V_{drop}| + |V_{stage}|$). (The stage velocity and its constancy during the impact are verified in the movies made to obtain the measurements.) The impact is imaged with a fast camera facing an intense collimated light source, which yields a sufficiently short time sampling (62 μs with a shutter time of 2 μs) and high spatial resolution (16 μm). A grazing view of the plate is used in order to access the whole deformation of the drop, including at the contact with the plate.

2.2. *General observations*

The typical impact dynamics for a concentrated suspension drop is illustrated in figure 1(*d*,*e*) for $\phi = 0.556$, $\eta_0 = 50.5$ mPa s and $V = 4$ m s^{-1}. As the drop makes contact with the plate, its lower surface flattens and the remainder of the drop widens while contracting in the vertical direction. The deformation is initially restricted to the region neighbouring the plate and progressively extends up to the top of the drop. The whole sequence lasts only a few hundreds of microseconds, after which all the kinetic energy is dissipated and fast deformations stop (the subsequent capillary–gravitational relaxation of the shape, lasting $\gtrsim$1 s and not shown in figure 1(*d*,*e*), is orders of magnitude slower).

We characterize the final spreading by measuring both the maximal diameter D_f and the contact diameter D_c (as observed from the side view, see figure 1*d*). This yields two different measurements of the deformation:

$$\beta \equiv \frac{D_f}{D_i} - 1 \quad \text{and} \quad \beta_c \equiv \frac{D_c}{D_{eq}}, \tag{2.1a,b}$$

where D_i and D_{eq} are, respectively, the maximal diameter before impact and the diameter of the equivalent-volume sphere. These definitions satisfy $\beta = \beta_c = 0$ for a vanishing deformation. To obtain the fairest comparison between the slightly different drop shapes, as well as with the spherical geometry assumed below, we choose to scale D_c by D_{eq} rather than D_i (which cannot be done for β since we require that it vanishes in the absence of deformation).

The dependence of the spreading on the particle volume fraction is presented in figure 2(*a*), for the same suspension and impact velocity as in figure 1(*d*). For both β and β_c the spreading decreases continuously and significantly from $\phi = 0$ up to the largest concentration explored here ($\phi = 0.587$). Importantly, the spreading is found to be almost unchanged upon using an impact plate with roughnesses of the order of d rather than a smooth glass plate. This suggests that, even with the smooth plate, there is no significant slipping of the particles at the plate surface.

Before seeking to understand the dependence to the particle content, a last crucial remark should be made by comparing the deformation obtained by varying both the

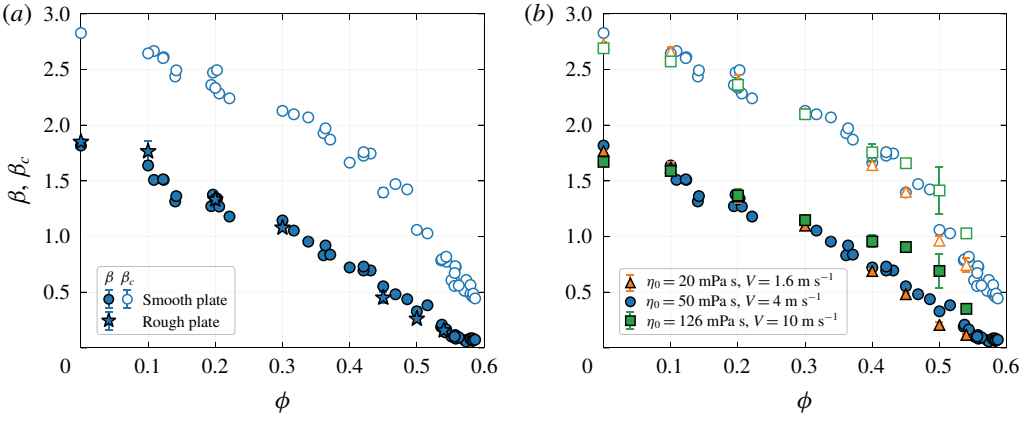

FIGURE 2. (*a*) Relative spreading as a function of the particle volume fraction for a suspension drop with $d = 145$ μm and $\eta_0 = 50.5$ mPa s ($V = 4$ m s^{-1}), as measured from the maximal deformed diameter D_f ($\beta \equiv D_f/D_i - 1$, filled symbols) and from the contact diameter D_c ($\beta_c \equiv D_c/D_{eq}$, open symbols). The error bars for $\phi = 0$, 0.1, 0.2, 0.3, 0.4, 0.45, 0.50 and 0.54 represent the standard deviation over three drop impacts. The other points represent a single impact event. (*b*) Spreading versus ϕ for different suspending liquids and the same ratio V/η_0.

velocity and suspending liquid such that the ratio V/η_0 remains constant, i.e. keeping the Reynolds number at fixed volume fraction unchanged. As shown in figure 2(*b*), the deformation is found to be essentially unchanged for a sixfold increase in V (with $Re_0 \equiv \rho V D_i/\eta_0 = 350 \pm 20$) over the whole range of ϕ. This suggests that, similarly to the Newtonian case and in contrast with the Bagnold scaling invoked in Boyer *et al.* (2016), the dissipation of the motion of the suspension drops follows a viscous scaling and is directly controlled by the Reynolds number.

To go beyond these findings and precisely assess the similarity and differences with the Newtonian case, a clear Newtonian reference is required, in particular in the limit of large viscosities (low Reynolds numbers), where the deformation is expected to be small.

3. Effective Newtonian approach

3.1. *Newtonian calibration and low-deformation limit*

The Newtonian reference is obtained by impacting drops of Newtonian liquids (PEGPG and UCON Oil (Dow) aqueous solutions, with a viscosity η between 0.012 and 41.5 Pa s) for values of $Re = \rho D_i V/\eta$ ranging from 10^{-1} to 10^3. As shown in figure 3(*a*), for large Re we recover the large-deformation limit, $\beta \sim Re^{1/5}$, derived by Madejski (1976). However, for larger viscosities, the deformation is so small that it is restricted to the surroundings of the contact with the plate (and no measurable oscillation of the diameter is observed). In this case we expect a different law. Assuming, in the spirit of Hertz's model for elastic deformations (Hertz 1896), that the deformed drop remains close to a sphere except for the flattened contact area with diameter $D_c \ll D_f \simeq D_i$ where it is indented with a typical depth $\delta \sim D_c^2/D_i$, one expects that the deformation is restricted to a volume $\Omega \sim D_c^3$ and has a typical magnitude $\varepsilon \sim \delta/D_c$. (This assumption is relevant in the present limit of $Re \lesssim 1$, for which the thickness of the viscous boundary layer, $\sim \sqrt{(\eta/\rho)t} \sim \sqrt{(\eta/\rho)D_c/V}$, is

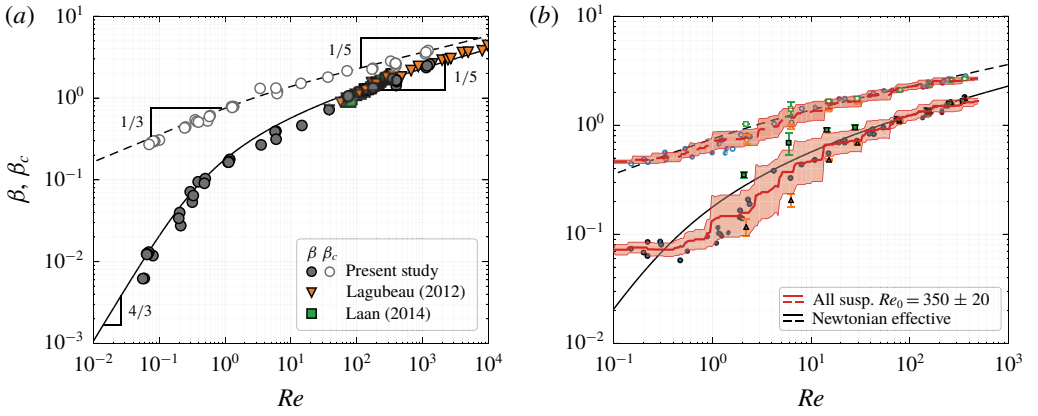

FIGURE 3. (*a*) Spreading for a viscous Newtonian drop as a function of the impact Reynolds number, $\rho D_i V/\eta_0$ (respectively, $\rho D_{eq} V/\eta_0$), for β (respectively, β_c). Six different PEGPG mixtures and pure UCON Oil are used. From large to low values of Re, the viscosity, velocity and Weber-number range, respectively, from 0.012 to 41.5 Pa s, from 4 to 0.4 m s^{-1} and from 2250 to 15 (the raw data are available at https://doi.org/10.1017/jfm.2020.394). The orange triangles represent the measurements of Lagubeau *et al.* (2012) (the value of $\beta = D_f/D_0 - 1 = (3h/2D_0)^{-1/2}$ is obtained from the relative thickness (h/D_0) they measure and from the assumption of a flat cylindrical shape of the deformed drop). The green squares represent those obtained by Laan *et al.* (2014) for the largest viscosity they have used ($\eta = 51$ mPa s). The lines represent equation (3.2). (*b*) The same data as in figure 2(*b*) plotted versus the effective Reynolds number $\rho D_i V/\eta(\phi)$ (respectively, $\rho D_{eq} V/\eta(\phi)$) for β (respectively, β_c) defined according to (3.3) with the critical volume fraction, $\phi_c = 0.605$, obtained with the indentation set-up (figure 4). The red line (respectively, envelope) represents a sliding geometrical average (respectively, standard deviation) of the spreading for the suspensions (the average is taken over $\pm$ one-third of a decade).

expected to be larger than the contact width D_c.) Equating the initial kinetic energy of the drop, $\sim \rho V^2 D_i^3$, with the viscous dissipation, $\sim \eta_0 \dot{\varepsilon} \varepsilon \Omega \sim \eta_0 \varepsilon^2 \Omega/(\delta/V)$, gives us $D_c/D_i \sim Re^{1/3}$. Last, making use of mass conservation, which imposes that the volume increase of the spherical part of the drop, ${D_f}^3 - {D_i}^3 \sim {D_i}^2(D_f - D_i)$, be equal to the indented volume, $\sim \delta D_c^2$, we obtain

$$\beta \equiv \frac{D_f}{D_i} - 1 \sim Re^{4/3} \quad \text{and} \quad \beta_c \equiv \frac{D_c}{D_{eq}} \sim Re^{1/3} \quad \text{for } Re \ll 1, \tag{3.1a,b}$$

which is found to be in good agreement with the measurements for small deformations (figure 3*a*). Note that, although the most viscous drops do not relax to a spherical shape before impact (similarly to the concentrated suspension drops), the two different definitions of the deformation yield the same agreement between (3.1) and the measurements, which suggests that the small departures from sphericity do not significantly affect the characterization of the deformation.

In order to allow the comparison between the suspension case and the Newtonian case for any deformation, we fit the Newtonian data with the following cross-over functions:

$$\left.\begin{aligned} Re \equiv F^{-1}(\beta) &= [(2\beta)^{3/16} + (1.4\beta)^{5/4}]^4, \\ Re \equiv {F_c}^{-1}(\beta_c) &= [(1.3\beta_c)^6 + (1.1\beta_c)^{10}]^{1/2}. \end{aligned}\right\} \tag{3.2}$$

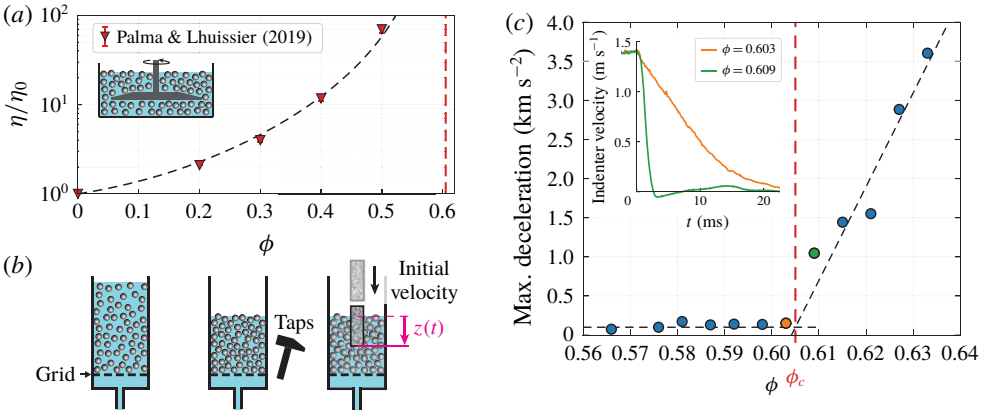

FIGURE 4. Rheological characterization of the suspensions. (*a*) Relative effective viscosity measured by Palma & Lhuissier (2019) for the same suspensions ($d = 145$ μm, PEGPG solution) as those used in the present study. The black dashed line is equation (3.3) with $a = 2.2$. The red dashed line indicates ϕ_c as measured in (*b*,*c*). (*b*) Indentation set-up used to measure the critical volume fraction ϕ_c. (*c*) Inset: decay of the indenter initial velocity for slightly different volume fractions of the sedimented particle pile ($t = 0$ indicates the contact instant). Main: maximal post-impact deceleration versus ϕ. The horizontal and inclined dashed lines are fitted to the data. Their intersection sets $\phi_c \simeq 0.605$.

These are plotted in figure 3(*a*) together with the measurements. Their functional form is chosen so as to recover the scaling laws of both the large- and the low-deformation limits.

In order to serve as a reference for the suspension case, this Newtonian formalism has to be complemented with a characterization of the effective rheology of the suspensions.

3.2. *Rheological characterization of the suspensions*

Figure 4(*a*) reports the bulk effective shear viscosity as a function of the particle volume fraction up to $\phi = 0.50$, as measured in one of our previous works for the same particles and liquids (Palma & Lhuissier (2019), the sketch of the dedicated shear cell used in this study is shown in the inset). To characterize the suspension at much higher volume fractions that cannot be accessed with the shear cell, we use a complementary protocol inspired by Jerome, Vandenberghe & Forterre (2016): a protocol of dynamic indentation into a sedimented state of the suspension, which allows us to measure accurately the critical volume fraction ϕ_c by probing the transient rheology both below and above ϕ_c. A sedimented particle pile is prepared at a volume fraction between $\simeq$0.565 and $\simeq$0.632 by letting the particle sediment gently at the loose random packing fraction $\simeq$0.565 and increasing the packing by a controlled tapping on the container (see figure 4*b*). The pile is indented dynamically with a solid cylinder impacting at 1.4 m s^{-1}. The post-impact velocity of the indenter is measured (with high precision by applying conventional image correlation methods to the speckle-patterned surface of the indenter), as shown in the inset of figure 4(*c*). For each value of ϕ, the maximal deceleration of the indenter is extracted. As shown in figure 4(*c*), the deceleration is almost constant (at typically 100 m s^{-2}) up to $\phi \simeq 0.605$, and increases significantly and almost linearly (by a factor up to 40), above.

This steep change in the transient rheology of the suspension indicates the onset of a dilatant response to deformation (Jerome *et al.* 2016), which implies an enhanced dissipation because the increase in pore volume between the particles forces a Darcy flow of the suspending liquid through the particle phase. By definition, the onset of dilatancy is also the maximal volume fraction at which a constant-volume deformation is possible, i.e. the volume fraction ϕ_c at which the steady effective rheology of the suspension diverges. We therefore obtain a direct and accurate characterization of ϕ_c for our suspensions by determining the onset of the dilatancy from the fitting procedure defined in the caption of figure 4(*c*), which yields $\phi_c \simeq 0.605$. This exhaustive characterization is obtained for $d = 145$ μm in pure water. However, by measuring the volume fraction of the loose random packing obtained by slow sedimentation (without tapping) we could verify that the value is almost the same (between 0.554 and 0.567) for all the different particles and suspending liquids that we have used, which indicates that the values of ϕ_c should also be almost the same. Similarly quasi-static measurements of the starting angle of avalanche in a rotating drum yielded very similar values for particles in water (25.5°) and in a 25 wt % PEGPG solution (27°).

To obtain an effective viscosity reference for the whole range of ϕ, we choose to summarize the above rheological characterizations by the following functional form:

$$\frac{\eta(\phi)}{\eta_0} = 1 + a - \frac{5\phi_c}{2} + \left(\frac{5\phi_c}{2} - 2a\right)\left[1 - \frac{\phi}{\phi_c}\right]^{-1} + a\left[1 - \frac{\phi}{\phi_c}\right]^{-2}, \tag{3.3}$$

where a is a fitting parameter. Similarly to Eilers' law (Stickel & Powell 2005), equation (3.3) verifies both Einstein relation ($\eta/\eta_0 \to 1 + 5\phi/2$) in the dilute limit and the inverse quadratic divergence ($\eta/\eta_0 \propto (\phi_c - \phi)^{-2}$) reported experimentally near ϕ_c. This ensures that (3.3) (with the fitted value $a = 2.2$) accurately represents the experimental data over the range $0 \leqslant \phi \leqslant 0.50$, as shown in figure 4(*a*), but also close to the critical volume fraction ϕ_c.

3.3. *Effective Newtonian deformation*

From the viscous spreading law, $\beta(\rho V D_i/\eta)$ (3.2), and the model for the steady effective viscosity of the suspensions, $\eta(\phi)$ (3.3), we obtain a prediction for the effective Newtonian spreading of a suspension drop as a function of the particle volume fraction:

$$\beta = F\left(\frac{\eta_0}{\eta(\phi)} Re_0\right) \quad \text{and} \quad \beta_c = F_c\left(\frac{\eta_0}{\eta(\phi)} Re_0\right), \tag{3.4a,b}$$

with $Re_0 = \rho V D_i/\eta_0$ and ρ stands for the density of the suspension. From the monotonic increase of $\beta(Re)$ and $\eta(\phi)$ and their low-Reynolds-number limits ($\beta \sim Re^{4/3}$, $\beta_c \sim Re^{1/3}$ and $\eta \propto (\phi_c - \phi)^{-2}$), equation (3.4) predicts that the deformation decreases with increasing ϕ and vanishes rapidly as the particle volume fraction approaches ϕ_c, according to $\beta \propto (\phi_c - \phi)^{8/3}$ and $\beta_c \propto (\phi_c - \phi)^{2/3}$. Consistently, equation (3.4) implies that the drop is not deformed at all above ϕ_c since the steady effective viscosity is infinite above ϕ_c.

We are now able to assess the relevance of the effective Newtonian approach to the suspension case. Figure 3(*b*) compares the same data as in figure 2 to equation (3.4). At low ϕ (large deformations and effective Reynolds numbers) the spreading of the suspensions is found to follow closely the effective Newtonian law. By contrast,

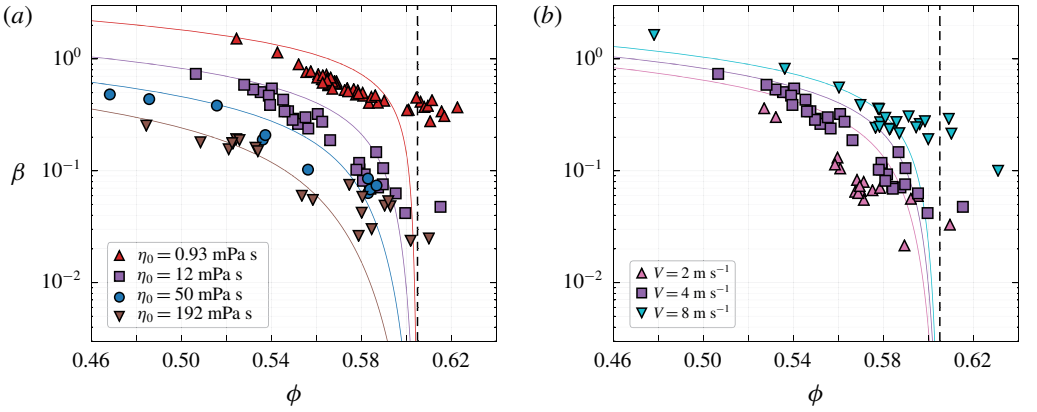

FIGURE 5. Spreading versus ϕ around the critical volume fraction ϕ_c for (*a*) different viscosities of the suspending liquid (at $V = 4$ m s^{-1}) and (*b*) varied impact velocities (for $\eta_0 = 12.0$ mPa s). The particle size is $d = 145$ µm. The coloured solid lines show the effective viscous law (2.1). The vertical dashed line indicates ϕ_c.

a significant departure is observed on the low-deformation side when the volume fraction approaches ϕ_c. Instead of continuing to decrease with decreasing effective Reynolds number, the spreading of the suspension seems to plateau or decrease much more slowly. (Although the spreading of purely Newtonian drops is still experimentally measurable and in agreement with the Newtonian law over this range of deformations; see figure 3*a*.)

4. Dilatancy effects and influence of the particle size

The measurements discussed above indicate a deviation from the effective Newtonian behaviour as ϕ becomes close to ϕ_c. Yet, although the deformation is not predicted any more by an effective Newtonian approach, experiments with volume fractions increased beyond ϕ_c confirm that the deformation remains controlled by a balance between inertia and viscous dissipation. As shown in figure 5(*a*,*b*), the spreading remains a decreasing function of the suspending liquid viscosity η_0 and an increasing function of the impact velocity V, including for ϕ above ϕ_c, where a finite deformation is observed, in stark contrast with the effective Newtonian expectation of a zero deformation.

The above observations suggest that at least one important aspect of the impact that is neglected by the effective Newtonian approach has to be considered to explain the spreading of very concentrated drops. Upon impact, the deformation of the particle phase, which determines the dissipation inside the suspension, does not necessarily proceed at a fixed volume fraction, in the sense of a fixed average distance between the particles. The volume of liquid and particles is conserved, but the particle phase can actually dilate by protruding from the liquid. As known since Reynolds' seminal demonstration of dilatancy (Reynolds 1885), this is actually the only way by which the drop can deform if it contains rigid particles at a volume fraction above ϕ_c. Direct observation confirms that the interface of the suspension becomes qualitatively more corrugated as the drop touches the plate and deforms (see e.g. figure 1*d*), but we are not able to quantify the effect because the protrusions are masking each other in the images.

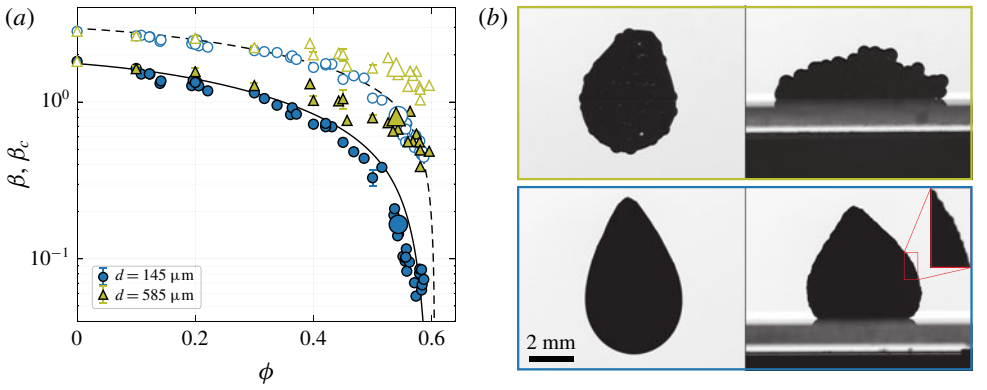

FIGURE 6. Influence of the particle size for the same suspending liquid and impact parameters ($\eta_0 = 50.5$ mPa s, $V = 4$ m s^{-1}). (*a*) Spreading versus ϕ (same data as in figure 2*a* for $d = 145$ μm). Filled (respectively, open) symbols correspond to β (respectively, β_c). (*b*) Comparison of the drop deformations for the same volume fraction $\phi = 0.54$ (larger symbols in (*a*), the scale is the same for the two concentrations).

Nevertheless, we can test the expected consequences of the dilatant motion. To fill the increasing volume between the diverging particles, the latter requires a Darcy flow of the suspending liquid through the particle phase (Jerome *et al.* 2016). For a dilatancy with a volume fraction decrease $-\Delta\phi \ll \phi$ one expects a dissipation per unit volume $\sim P\Delta\phi/\phi$, where the pore pressure P built up by the Darcy flow follows $-P/D_i^2 \sim (1/\kappa)\eta_0\dot{\varepsilon}(\Delta\phi/\phi) \sim (1/\kappa)\eta_0 V/D_i(\Delta\phi/\phi)$ and $\kappa \sim 10^{-3}d^2$ is the typical permeability of the particle phase at high solid fractions. In the limit of very small deformations and $\phi \gtrsim \phi_c$, the dilatancy may be assumed to be slaved to the deformation, i.e. $-\Delta\phi/\phi \sim \beta$, and the deformation should be limited by the dissipation of the dilatant motion, i.e. $P\Delta\phi/\phi \sim \rho V^2$. This assumption is found to be compatible with experiments. For the experimental values $d = 145$ μm, $\eta_0 = 50.5$ mPa s, $V = 4$ m s^{-1} and the typical saturation deformation observed at very high concentration, $\beta \sim 3 \times 10^{-2}$ (see figure 5), the estimated dissipation of the dilatant motion, $P\Delta\phi/\phi \sim (1/\kappa)\eta_0 V D_i \beta^2 \sim 10^4$ Pa, is indeed found to be of the same order as the stagnation pressure ρV^2.

This scaling analysis, which neglects the details of the impact geometry and assumes uniform deformation and dilatation, is too simple to explain quantitatively all the experimental data. However, it explains qualitatively why the deformation remains controlled by V and η_0 for $\phi \gtrsim \phi_c$. Furthermore, it predicts a crucial dependence of the deformation of the drop at large concentrations, namely, that the deformation should increase with increasing permeability of the solid phase, i.e. with increasing particle size. This dependence on d is tested experimentally in figure 6(*a*), which compares the spreadings measured for $d = 585$ μm together with those obtained with $d = 145$ μm for the same viscosity and impact velocity ($\eta_0 = 50.5$ mPa and $V = 4$ m s^{-1}). Although the spreadings are similar at low volume fractions ($\phi \lesssim 0.30$), it is found to be significantly larger for the larger particles at higher concentrations (in terms of both β and β_c). As illustrated more directly from the images in figure 6(*b*) for $\phi = 0.54$, for both $d = 585$ μm and $d = 145$ μm the two drops become more corrugated during the impact, which shows that in both cases the particle phase dilates. Yet, the drop with the larger particles deforms and spreads significantly more, as expected from a deformation limited by dilatancy.

5. Conclusions

We have considered the impact of a drop loaded with solid particles with the aim of describing the high-volume-fraction limit ($\phi \gtrsim \phi_c$), where a viscous effective approach predicts a vanishing deformation. A careful characterization of (i) the bulk effective viscosity of our suspensions and (ii) the low-deformation limit of a viscous impact has provided us with a precise effective Newtonian reference. While the spreading of the suspension drop measured at moderate volume fractions is in agreement with the latter, a clear deviation is observed for larger values of ϕ. In particular, a finite deformation is actually observed above ϕ_c, in contradiction with the effective approach. This suggests that, although there is no splashing or particle ejection, the volume fraction of the suspension – in terms of the mean distance between the particles – is not fixed during the impact, which is consistent with the dilatant motion of the particle phase observed during the impact. The deformation around ϕ_c is found to depend on the particle size, not only above ϕ_c but also slightly below, with larger deformations observed for larger particles. This dependence cannot be attributed to a capillary effect related with the size of the menisci between the outermost particles, since the deformation is found to remain controlled by the viscosity of the suspending liquid for all values of ϕ. This suggests that the observed dependence on the particle size is actually related with the dilatant motion itself, because dilatancy drives a Darcy flow that is all the more dissipative when the suspending liquid is viscous and the particles are small. This also means that a complete description of the impact of concentrated suspension drops will require one to combine the unsteady surface flow facet of the problem with a two-phase approach that can account for variations of the solid volume fraction and for the associated transient dissipation.

Acknowledgement

This work has been financially supported by the Agence Nationale de la Recherche through grant ANR-14-ACHN-0019-01.

Declaration of interests

The authors report no conflict of interest.

Supplementary movies

Supplementary movies are available at https://doi.org/10.1017/jfm.2020.394.

References

BERTOLA, V. & HAW, M. 2015 Impact of concentrated colloidal suspension drops on solid surfaces. *Powder Technol.* **270**, 412–417.

BOYER, F., SANDOVAL-NAVA, E., SNOEIJER, J., DIJKSMAN, J. & LOHSE, D. 2016 Drop impact of shear thickening liquids. *Phys. Rev. Fluids* **1**, 013901.

CHANDRA, S. & AVEDISIAN, C. 1991 On the collision of a droplet with a solid surface. *Proc. R. Soc. Lond.* A **432**, 13–41.

DERBY, B. 2011 Inkjet printing ceramics: from drops to solid. *J. Eur. Ceram. Soc.* **31**, 2543–2550.

GORDILLO, L., SUN, T.-P. & CHENG, X. 2018 Dynamics of drop impact on solid surfaces: evolution of impact force and self-similar spreading. *J. Fluid Mech.* **840**, 190–214.

GRISHAEV, V., IORIO, C., DUBOIS, F. & AMIRFALZI, A. 2015 Complex drop impact morphology. *Langmuir* **31**, 9833–9844.

GUAZZELLI, É. & POULIQUEN, O. 2018 Rheology of dense granular suspension. *J. Fluid Mech.* **852**, P1.

HERTZ, H. 1896 On the contact of elastic solids. *J. Reine Angew. Math.* **92**, 156–171.

INGOLD, C. 1971 *Fungal Spores. Their Libération and Dispersal*. Clarendon.

JEROME, J., VANDENBERGHE, N. & FORTERRE, Y. 2016 Unifying impacts in granular matter from quicksand to cornstarch. *Phys. Rev. Lett.* **117**, 098003.

JOSSERAND, C. & THORODDSEN, S. 2016 Drop impact on a solid surface. *Annu. Rev. Fluid Mech.* **48**, 365–391.

KORKUT, S., SAVILLE, D. & AKSAY, I. 2008 Collodial cluster arrays by electrohydrodynamic printing. *Langmuir* **24**, 12196–12201.

LAAN, N., DE BRUIN, K., BARTOLO, D., JOSSERAND, C. & BONN, D. 2014 Maximum diameter of impacting liquid droplets. *Phys. Rev. Appl.* **2**, 044018.

LAGUBEAU, G., FONTELOS, M., C, J., MAUREL, A., PAGNEUX, V. & PETITJEANS, P. 2012 Spreading dynamics of drop impacts. *J. Fluid Mech.* **713**, 50–60.

LUBBERS, L., XU, Q., WILKEN, S., ZHANG, W. & JAEGER, H. 2014 Dense suspension splat: monolayer spreading and hole formation after impact. *Phys. Rev. Lett.* **113**, 044502.

MADEJSKI, J. 1976 Solidification of droplets on a surface. *Intl J. Heat Mass Transfer* **19**, 1009–1013.

MORRIS, J. 2020 Spreading dynamics of drop impacts. *Annu. Rev. Fluid Mech.* **52**, 121–144.

NICOLAS, M. 2005 Spreading of a drop of neutrally buoyant suspension. *J. Fluid Mech.* **545**, 271–280.

PALMA, S. & LHUISSIER, H. 2019 Dip-coating with a particulate suspension. *J. Fluid Mech.* **869**, R3.

PETERS, I., XU, Q. & JAEGER, H. 2013 Splashing onset in dense suspension droplets. *Phys. Rev. Lett.* **111**, 028301.

QI, L., MCMURRY, P., NORRIS, D. & GIRSHICK, S. 2011 Impact dynamics of colloidal quantum dot solids. *Langmuir* **27**, 12677–12683.

RAUX, P., TROGER, A., JOP, P. & SAURET, A. 2020 Spreading and fragmentation of particle-laden liquid sheets. *Phys. Rev. Fluids* **5**, 044004.

REYNOLDS, O. 1885 On the dilatancy of media composed of rigid particles in contact, with experimental illustrations. *Phil. Mag.* **20**, 449–481.

SCHAARSBERG, M., PETERS, I., STERN, M., DODGE, K., ZHANG, W. & JAEGER, H. 2016 From splashing to bouncing. *Phys. Rev.* E **93**, 062609.

STICKEL, J. & POWELL, R. 2005 Fluid mechanics and rheology of dense suspensions. *Annu. Rev. Fluid Mech.* **37**, 129–149.

WILDEMAN, S., VISSER, C. W., SUN, C. & LOHSE, D. 2016 On the spreading of impacting drops. *J. Fluid Mech.* **805**, 636–655.

ZARRAGA, I., HILL, D. & LEIGHTON, D. 2000 The characterization of the total stress of concentrated suspensions of noncolloidal spheres in Newtonian fluids. *J. Rheol.* **44**, 185–220.